Search Method of Robust Gate Driving Vectors for Digital Gate Drivers With Low Test Cost Against Load Current and Temperature Variations in IGBTs

Ting-Wei Wang, *Student Member, IEEE*, Toshiaki Inuma, Po-Hung Chen, *Senior Member, IEEE*, and Makoto Takamiya, *Senior Member, IEEE*

***Abstract*—A digital gate driver with active gate driving is effective in solving the tradeoff between switching loss and current/voltage overshoot of power devices. However, the optimum gate driving vector (GV) for a digital gate driver is temperature- and load current-dependent. When an optimum GV at a particular operating condition is reused to another, the switching performance sometimes becomes worse than the conventional gate drive (Sai et al. 2019). Therefore, robust gate driving vectors (RGVs) against temperature and load current variation are required (Sai et al. 2019). Nevertheless, the test cost of searching for an RGV is very high. In order to reduce the test cost, search methods of RGV with fewer required measurements are proposed in this article. Single-step GV and stop-and-go GV are selected as the type of RGV for turn-ON and turn-OFF, respectively. Compared with the conventional search method of RGV in Sai et al. 2019 and Wang et al. 2020, the proposed search method can reduce the measurement time by 99% and 92%, respectively. Furthermore, when the RGV and the optimum GV at a single condition are reused to other operating conditions, the maximum overall f_{OBJ} of RGV is lower than that of the single condition optimum GV, which shows that the searched RGV has better robustness.**

***Index Terms*—Gate driver, insulated gate bipolar transistor (IGBT), load current, robustness, temperature.**

I. Introduction

INSULATED gate bipolar transistors (IGBTs) have been widely employed in high-power applications due to their high voltage/current capability and ease of driving. In a power system, the gate driver acts as the interface between low-voltage control signals and power devices such as IGBTs. Therefore, the gate driver has a direct impact on the switching behavior of IGBTs. Conventional gate drivers (CGDs) adopt fixed gate drive voltage and fixed gate resistance to control the charging of the IGBT's gate capacitance throughout entire switching periods. Generally, the gate drive voltage or resistance is selected to meet requirements such as switching loss, overshoots and electromagnetic interference. Unfortunately, CGD cannot achieve a compromise between these conflicting objectives simultaneously. To overcome the drawback of CGD, many works of active gate driver (AGD) have been proposed [1], [2], [3], [4], [5], [6], [7], [8], [9], [10], [11], [12], [13], [14], [15], [16], [17], [18], [19], [20], [21], [22], [23], [24], [25], [26], [27], [28], [29], [30], [31], [32], [33], [34], [35], [36], [37], [38], [39]. Active gate driving of power devices, where the gate driving current is dynamically controlled during the turn-ON/OFF transients, is a solution to solve the trade-off between the switching loss (E_{LOSS}) and the current overshoot ($I_{\mathrm{OVERSHOOT}}$) or the voltage overshoot ($V_{\mathrm{OVERSHOOT}}$) of CGD. The AGD technique reported in [2], [3], [4], and [5] is composed of a fixed voltage source and switched resistors to control the gate charging current. Multilevel AGDs are introduced in [6], [7], [8], [9], and [10]. The gate driving voltage is changed at different stages during the switching transients. Analog controller-based current source presented in [11], [12], [13], [14], and [15] is a common method for gate driving current adjustment in AGD. In addition, active gate driving can also be realized by a digital gate driver [16], [17], [18], [19], [20], [21], [22], [23], [24], [25], [26], [27], [28], [29], [30], [31], [32], [33], [34], [35], [36], [37], [38], [39] as the gate driving current of a digital gate driver is programmable with gate driving vectors (GVs). As depicted in Fig. 1, GV represents the gate driving pattern

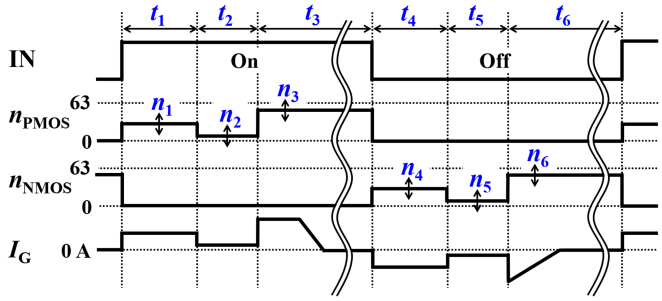

Fig. 1. Example of GV.

Manuscript received 14 January 2023; revised 31 March 2023; accepted 16 May 2023. Date of publication 24 May 2023; date of current version 28 July 2023. This work was supported in part by the National Science and Technology Council, Taiwan, under Grant 111-2636-E-A49-009 and in part by the Higher Education Sprout Project of the National Yang Ming Chiao Tung University and Ministry of Education, Taiwan. Recommended for publication by Associate Editor A. Lindemann. *(Corresponding author: Po-Hung Chen.)*

Ting-Wei Wang and Po-Hung Chen are with the Institute of Electronics, National Yang Ming Chiao Tung University, Hsinchu 30010, Taiwan (e-mail: twwang.ee06g@nctu.edu.tw; hakko@nycu.edu.tw).

Toshiaki Inuma and Makoto Takamiya are with the Institute of Industrial Science, The University of Tokyo, Tokyo 153-8505, Japan (e-mail: inuma@iis.u-tokyo.ac.jp; mtaka@iis.u-tokyo.ac.jp).

Color versions of one or more figures in this article are available at https://doi.org/10.1109/TPEL.2023.3279674.

Digital Object Identifier 10.1109/TPEL.2023.3279674

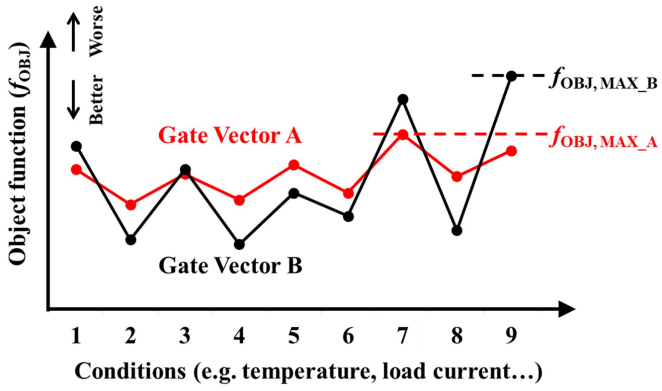

Fig. 2. Concept of RGV.

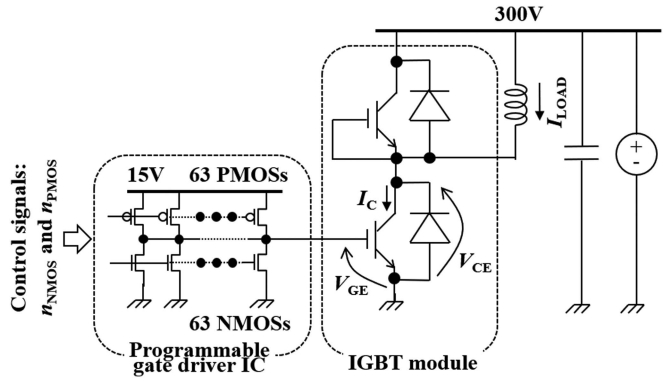

Fig. 3. Circuit schematic of measurement setup.

of a digital gate driver. GV is composed of several steps n and their durations t, where the gate charging/discharging current is positively correlated to the magnitude of n. For example, a 6-b programmable digital gate driver with four 6-bit variables for IGBT is proposed in [16]. The optimum GV is automatically found out of 64^4 ($\sim 1.7 \times 10^7$) combinations by more than 2000 measurements using a simulated annealing (SA) algorithm. As a result, the E_{LOSS} is reduced by 55% at the same $V_{\mathrm{OVERSHOOT}}$, and the $V_{\mathrm{OVERSHOOT}}$ is reduced by 53% at the same E_{LOSS} at the turn-OFF of IGBT. However, the optimum GV varies depending on operating conditions such as temperature and load current (I_{LOAD}) [17]. When an optimum GV at a particular temperature and I_{LOAD} is reused to another temperature and I_{LOAD}, the E_{LOSS} and $I_{\mathrm{OVERSHOOT}}/V_{\mathrm{OVERSHOOT}}$ of IGBT are sometimes worse than the conventional single-step gate drive [17]. Therefore, robust gate driving vectors (RGV) against temperature and I_{LOAD} variations are required to solve the problem [18].

The concept of RGV is illustrated in Fig. 2. The object function (f_{OBJ}) is a function of E_{LOSS} and $I_{\mathrm{OVERSHOOT}}/V_{\mathrm{OVERSHOOT}}$ of IGBT during turn-ON/OFF transient. The f_{OBJ} is used to estimate the performance in the SA algorithm [19]. A smaller f_{OBJ} shows better performance on E_{LOSS} and $I_{\mathrm{OVERSHOOT}}/V_{\mathrm{OVERSHOOT}}$. RGVs are universal GVs that can be applied to different operating conditions. Although RGV may not have an outstanding f_{OBJ} under a specific optimization condition, it reduces the maximum f_{OBJ} across different operating conditions. Take the two GVs in Fig. 2 for example, the $f_{\mathrm{OBJ,\ MAX\cdot A}}$ is lower than the $f_{\mathrm{OBJ,\ MAX\cdot B}}$, which indicates that the gate vector A has better robustness than the gate vector B. From a practical viewpoint, product specifications are often determined by the maximum f_{OBJ}, which makes minimizing the maximum f_{OBJ} across variations in operating conditions important. However, the test cost of searching for an RGV is very high. In [18], 90 000 measurements for a full search of GVs across nine different temperature and I_{LOAD} are required to search an RGV, which take more than 5.5 h. To reduce the test cost, robust simulated annealing (RSA) for an automatic search method of RGV against temperature variation is described in [20]. Nonetheless, RGV against I_{LOAD} variation is not included.

In this article, search methods of RGVs with low test costs are proposed. Different types of GVs are chosen for RGV in turn-ON and turn-OFF states. Compared with the conventional full search method of RGV [18] and RSA [20], the proposed search method of RGV has the lowest test cost. Moreover, when the searched RGV and the optimum GV at single condition are both reused to other temperature and I_{LOAD} conditions, the maximum overall f_{OBJ} of RGV is lower than that of the single condition optimum GV, demonstrating the stronger robustness of the searched RGV.

The other sections of this article are organized as follows. The proposed RGV search methods for turn-ON and turn-OFF are introduced in Section II. In Section III, the measurement results are shown. Section IV describes the comparison between the proposed RGV and previous works. Finally, Section V presents the conclusion drawn from this article.

II. RGV Search Method

In this section, the measurement setup and different types of GVs are introduced. Then, the single-step GV and the stop-and-go GV in both turn-ON and turn-OFF states are discussed. Furthermore, the proposed search methods of RGV for turn-ON and turn-OFF are described in detail, respectively.

A. Measurement Setup and Gate Driving Vector

Fig. 3 shows a circuit schematic of the double pulse test measurement setup for the turn-ON and turn-OFF of IGBT at 300 V. The measurement system consists of a 6-b programmable digital gate driver [19], a 2-in-1 IGBT module (2MBI100TA-060- 50, 600 V, 100 A), and a signal acquisition/control system. In order to realize a programmable 63-level drivability in the programmable digital gate driver, 63 parallel transistors are connected to the gate of IGBT, and a 6-bit control signal is applied to specify the number of activated PMOS (NMOS) transistors, n_{PMOS} (n_{NMOS}) [19].

Fig. 4 shows the GVs and waveforms for turn-ON state in the 6-bit digital gate driver. Fig. 4(a) shows the single-step GV and Fig. 4(b) shows the stop-and-go GV. The single-step GV can be expressed as (n), where n is an integer from 1 to 63. In order to increase the gate charge resolution of conventional stop-and-go GV [21] in a specific range, n_1 is fixed to 25, and thereby n_2 is

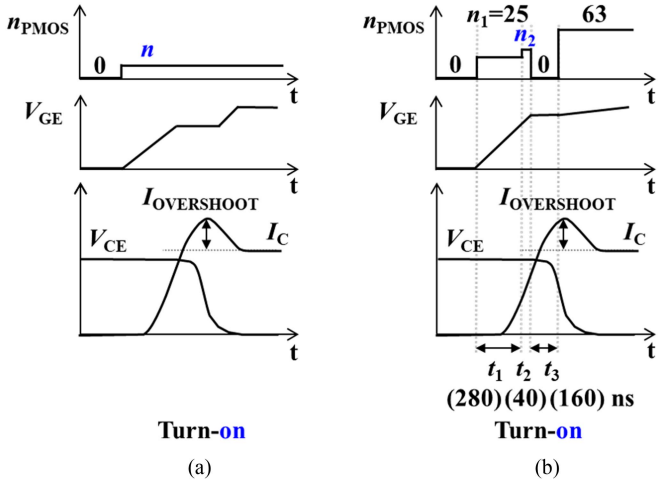

Fig. 4. GVs and waveforms in turn-ON state. (a) Single-step gate drive. (b) Stop-and-go gate drive.

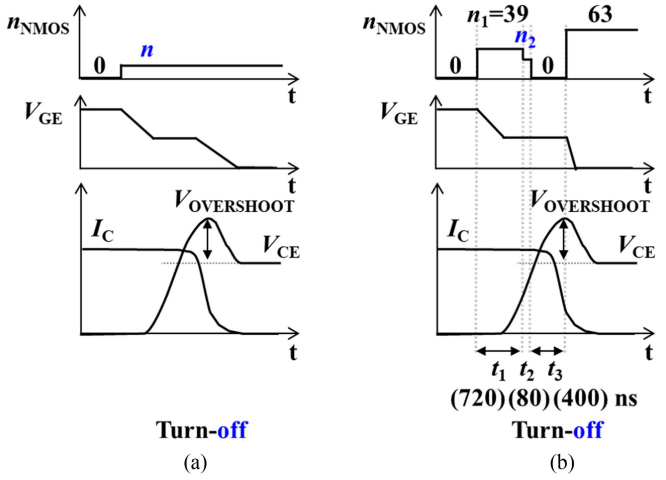

Fig. 5. GVs and waveforms in turn-OFF state. (a) Single-step gate drive. (b) Stop-and-go gate drive.

the only variable. Thus, the stop-and-go GV for turn-ON in this article is defined as (25, n_2, 0, 63), where n_2 is an integer from 0 to 63.

Fig. 5 shows the GVs and waveforms for turn-OFF state in the 6-b digital gate driver. Fig. 5(a) shows the single-step GV, and Fig. 5(b) shows the stop-and-go GV. The single-step GV can be expressed as (n), where n is an integer from 1 to 63. The purpose of Fig. 5(b) is the same as Fig. 4(b), which is for higher gate charge resolution. Thus, the stop-and-go GV for turn-OFF in this article is defined as (39, n_2, 0, 63), where n_2 is an integer from 0 to 63. The selection of n_1, t_1 and t_3 in stop-and-go GV of turn-ON and turn-OFF states are described in [21]. The t_2 is set 10% of the total duration of t_1 and t_2.

To evaluate the performance of a GV, the turn-ON object function (f_{OBJ_ON}) and turn-OFF object function (f_{OBJ_OFF}) are defined as

$$f_{OBJ\_ON} = \sqrt{\left(\frac{E_{LOSS}}{E_{LOSS,\,MAX}}\right)^2 + \left(\frac{I_{OVERSHOOT}}{I_{OVERSHOOT,\,MAX}}\right)^2} \quad (1)$$

$$f_{OBJ\_OFF} = \sqrt{\left(\frac{E_{LOSS}}{E_{LOSS,\,MAX}}\right)^2 + \left(\frac{V_{OVERSHOOT}}{V_{OVERSHOOT,\,MAX}}\right)^2} \quad (2)$$

where the subscript MAX signifies the maximum of the corresponding quantity. The $E_{LOSS,\,MAX}$, $I_{OVERSHOOT,\,MAX}$, and $V_{OVERSHOOT,\,MAX}$ terms in (1) and (2) are determined by the measured results of single-step GVs, which are labeled in Figs. 12 and 13.

In this article, to explain the proposed RGV search method, E_{LOSS} and $I_{OVERSHOOT}$ /$V_{OVERSHOOT}$ of IGBT are measured across nine conditions, including different I_{LOAD} (20 A, 50 A, 80 A) and temperature (25 °C, 75 °C, 125 °C).

B. Proposed Search Method of Robust Single-Step GV in Turn-ON

Fig. 6(a) shows the measured f_{OBJ} versus n with single-step GV at nine different I_{LOAD} and temperature conditions in turn-ON state. Fig. 7(a) shows the measured f_{OBJ} versus n_2 with stop-and-go GV at nine conditions in turn-ON state. The target is to search for a single n/n_2 with the lowest maximum f_{OBJ}. Comparing the maximum f_{OBJ} curve of two GVs in Figs. 6(b) and 7(b), single-step GV gives a lower maximum f_{OBJ}, which shows a better switching performance. Therefore, single-step GV is selected as the type of RGV for turn-ON.

To search the robust single-step (RSS) GV (n), a worst-case search method is used. In Fig. 6(a), the case of 80 A, 125 °C provides the largest f_{OBJ}s among almost all different n. In other words, the case of 80 A, 125 °C decides the maximum f_{OBJ} of the nine conditions with every single n, which shows that 80 A, 125 °C is the worst case of the nine conditions. Therefore, we can search the RGV at 80 A, 125 °C instead of nine different conditions. Then, $n = 13$ with the lowest f_{OBJ} at 80 A, 125 °C is found as the target RGV.

As stated above, single-step GV is chosen as the RGV type for turn-ON. The proposed RSS GV search method is to search the optimum n at the condition of largest I_{LOAD} and highest temperature. Therefore, only 63 measurements are required to search the RGV with the proposed search method, which results in reduced test cost. If stop-and-go is selected as the RGV type, test cost is increased to 567 ($= 9 \times 63$) measurements.

C. Proposed Search Method of Robust Stop-and-Go GV in Turn-OFF

Fig. 8(a) shows the measured f_{OBJ} versus n with single-step GV at nine different I_{LOAD} and temperature conditions in turn-OFF state. Fig. 9(a) shows the measured f_{OBJ} versus n_2 with stop-and-go GV at nine conditions in turn-OFF. Comparing the maximum f_{OBJ} curve of two GVs in Figs. 8(b) and 9(b), stop-and-go GV gives a lower maximum f_{OBJ}, which shows a better switching performance. Hence, stop-and-go GV is more suitable as the type of RGV for turn-OFF.

Fig. 10 shows the optimum n_2 extracted from Fig. 9(a) at nine different I_{LOAD} and temperature conditions. As the I_{LOAD} increases, n_2 slightly reduces. As the temperature increases, n_2 increases significantly. Therefore, n_2 shows both I_{LOAD} and

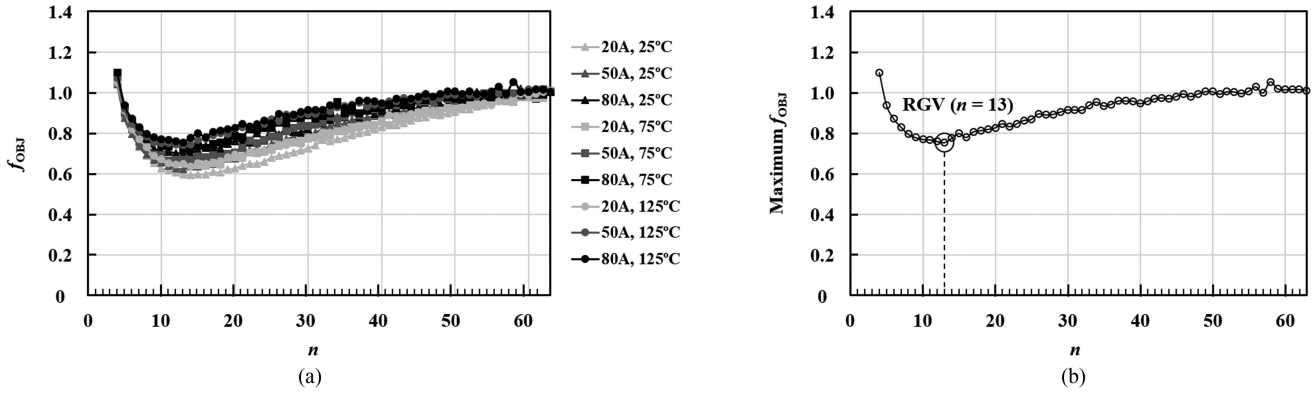

Fig. 6. Single-step gate drive in turn-ON state. (a) f_{OBJ} versus n of nine conditions. (b) Maximum f_{OBJ} vs. n.

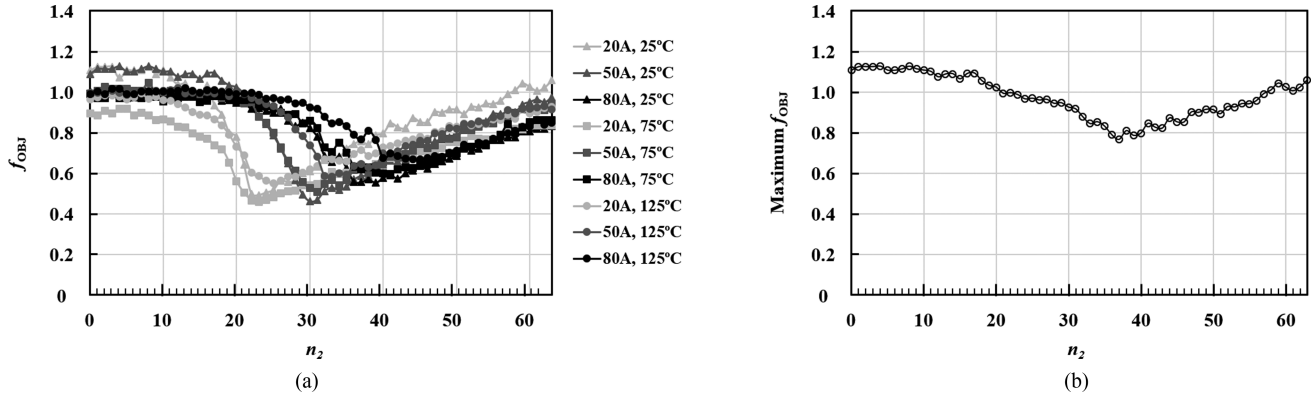

Fig. 7. Stop-and-go gate drive in turn-ON state. (a) f_{OBJ} versus n_2 of nine conditions. (b) Maximum f_{OBJ} vs. n_2.

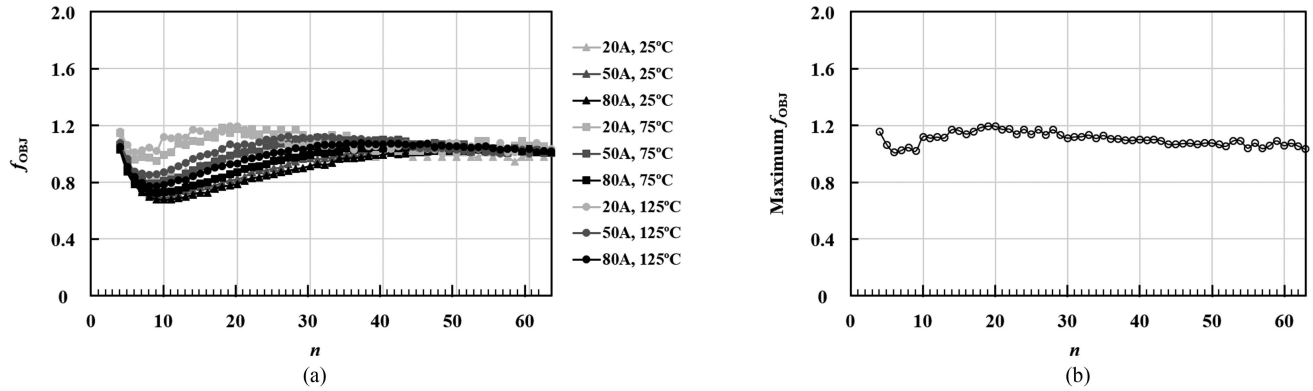

Fig. 8. Single-step gate drive in turn-OFF state. (a) f_{OBJ} versus n of nine conditions. (b) Maximum f_{OBJ} versus n.

temperature correlation. The four corner conditions are defined as (the smallest and largest I_{LOAD}) $\times$ (the lowest and highest temperature). The results of the four corner conditions include that of the nine conditions. Fig. 11 shows the maximum f_{OBJ} curve at four corner conditions, similar to Fig. 9(b).

From Fig. 9(a), for any condition, when n_2 is smaller than the optimum value, the f_{OBJ} increases significantly, which indicates worse switching performances of E_{LOSS} and $V_{\mathrm{OVERSHOOT}}$. In other words, the targeting region is where n_2 is larger than the optimum value.

As stated above, a search method of robust stop-and-go (RSNG) GV for turn-OFF is proposed. There are two steps in the search method introduced in the following.

1) Search optimum n_2 under each corner condition of I_{LOAD} and temperature. Since n_2 shows both I_{LOAD} and temperature correlation, the searching range can be set to

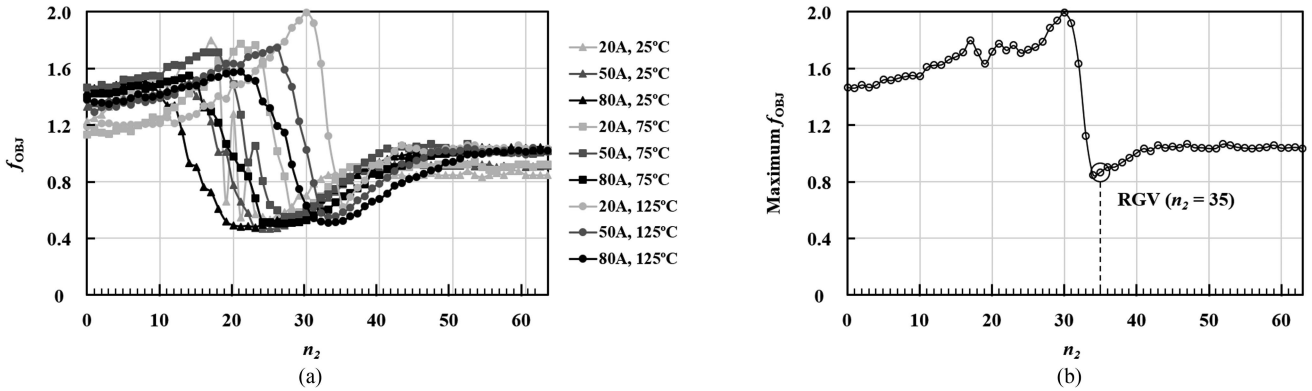

Fig. 9. Stop-and-go gate drive in turn-OFF state. (a) f_{OBJ} versus n_2 of nine conditions. (b) Maximum f_{OBJ} versus n_2.

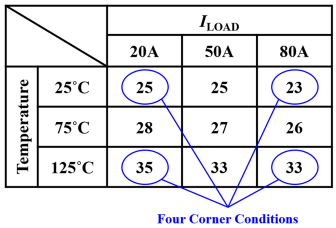

Fig. 10. Optimum n_2 of stop-and-go gate drive across nine conditions including different I_{LOAD} and temperature.

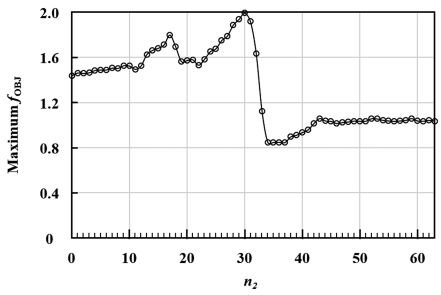

Fig. 11. Maximum f_{OBJ} versus n_2 of stop-and-go gate drive in turn-OFF state at four corner conditions.

corner condition instead of full search under all operating conditions.

2) Choose the largest optimum n_2 from four corner conditions as the target n_2 and thus the RSNG GV is found. The reason for choosing the largest n_2 is to make sure that the chosen n_2 is in the target region of other operating conditions.

By using the proposed search method, a largest $n_2 = 35$ can be found at 20 A, 125 °C, and therefore the RSNG GV for turn-OFF is searched. A total of 256 ($= 4 \times 64$) measurements are required to search the RGV with the proposed search method, which results in reduced test cost.

III. Measured Results

In order to clarify that the RGVs from the proposed search method are effective in providing smaller maximum f_{OBJ}s, E_{LOSS} and $I_{\mathrm{OVERSHOOT}}/V_{\mathrm{OVERSHOOT}}$ of IGBT are measured across nine conditions including different I_{LOAD} (20 A, 50 A, 80 A) and temperature (25 °C, 75 °C, 125 °C). Fig. 12 shows the measured E_{LOSS} versus $I_{\mathrm{OVERSHOOT}}$ of different gate drives in turn-ON state, while Fig. 13 shows the measured E_{LOSS} versus $V_{\mathrm{OVERSHOOT}}$ in turn-OFF state. The black curves show the tradeoff of the single-step gate drive with varied n from 4 to 63. The black circles show the RSS gate drive searched with the proposed search method, where $n = 13$ in turn-ON state. The blue curves show the results of the stop-and-go gate drive with varied n_2 from 0 to 63. The blue circles show the RSNG GV searched with the proposed search method, where $n_2 = 35$ in the turn-OFF state. The red circles show the reuse of optimum stop-ang-go GV at 50 A, 75 °C. The dotted concentric curves show the contour of $f_{\mathrm{OBJ\_ON}}$ and $f_{\mathrm{OBJ\_OFF}}$ defined in (1) and (2), respectively. The f_{OBJ}s of the abovementioned gate drives at nine conditions in turn-ON and turn-OFF state are respectively plotted in Fig. 14(a) and (b). The maximum f_{OBJ}s of the RGVs with the proposed search method are the lowest, which indicates that the concept of robustness is realized.

A. Turn-ON

Fig. 15(a)–(c) show the GVs and the measured waveforms in turn-ON state at 50 A, 75 °C of the RSS GV ($n = 13$), the RSNG GV ($n_2 = 37$) and the optimum stop-and-go GV ($n_2 = 31$), respectively. The optimum stop-and-go GV gives the best switching performance among the three different GVs.

Fig. 16(a)–(c) show the GVs and the measured waveforms in turn-ON state at 80 A, 125 °C of the RSS GV ($n = 13$), the RSNG GV ($n_2 = 37$) and the reuse of optimum stop-and-go GV ($n_2 = 31$) at 50 A, 75 °C, respectively. As clearly shown in the extracted result from Fig. 14(a), the proposed RSS GV gives the lowest maximum f_{OBJ} across the nine conditions. In contrast, the reuse of stop-and-go GV gives a larger f_{OBJ} than the RGVs. Therefore, the reuse of an optimum GV is not robust to I_{LOAD} and temperature variations.

B. Turn-OFF

Fig. 17(a)–(c) show the GVs and the measured waveforms in turn-OFF state at 50 A, 75 °C of the RSS GV ($n = 6$),

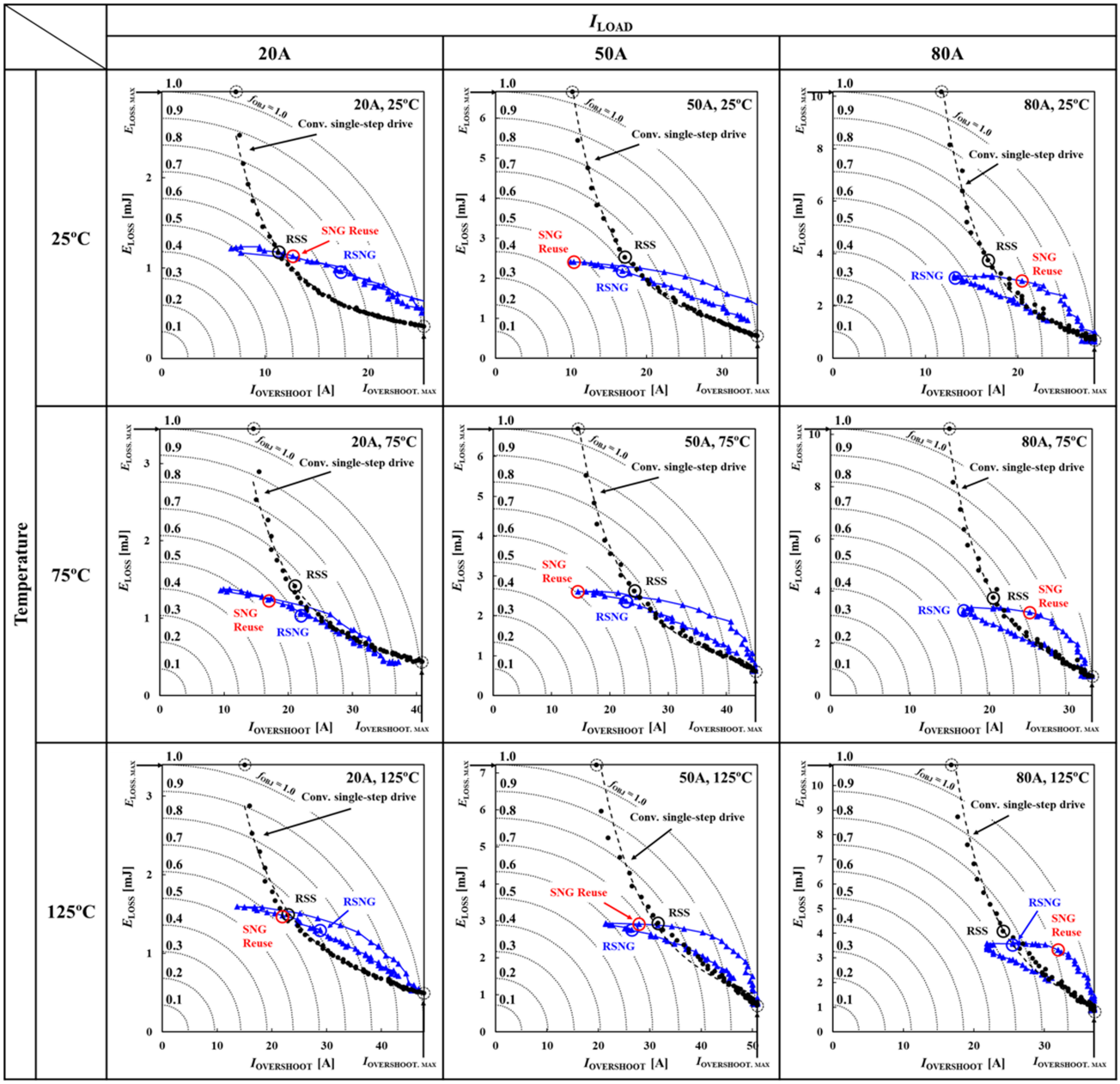

Fig. 12. Measured E_{LOSS} versus $I_{\mathrm{OVERSHOOT}}$ of different gate drives in turn-ON state. Black curves: tradeoff curves of single-step gate drive with varied n. Blue curves: results of stop-and-go gate drive with varied n_2. Black circles: proposed robust single-step gate drive (RSS). Blue circles: robust stop-and-go (RSNG) gate drive. Red circles: reuse of optimum stop-and-go GVs at 50 A, 75 °C (SNG reuse).

the RSNG GV ($n_2 = 35$) and the optimum stop-and-go GV ($n_2 = 27$), respectively. The optimum stop-and-go GV gives the best switching performance among the three different GVs.

Fig. 18(a)–(c) show the GVs and the measured waveforms in turn-OFF state at 20 A, 125 °C of the RSS GV ($n = 6$), the RSNG GV ($n_2 = 35$) and the reuse of optimum stop-and-go GV ($n_2 = 27$) at 50 A, 75 °C, respectively. As clearly shown in the extracted result from Fig. 14(b), the reuse of stop-and-go GV gives a larger f_{OBJ} than the RGVs. Therefore, the reuse of an optimum GV is not robust to I_{LOAD} and temperature variations. As shown in Fig. 14(b), the proposed RSNG GV gives the lowest maximum f_{OBJ} across the nine conditions, which shows that the proposed RGV is effective to both I_{LOAD} and temperature variations.

IV. Discussion

Different search methods and different types of RGVs were proposed in [18] and [20]. In this section, the test cost and performance of the proposed RGVs are discussed and compared with previous RGV works.

In [18], a full search across nine conditions is used to find the RGV. The GV is defined as (n_1, n_2, n_3, n_4). To reduce the combinations of GV, the levels of n_1, n_2, n_3 and n_4 are reduced

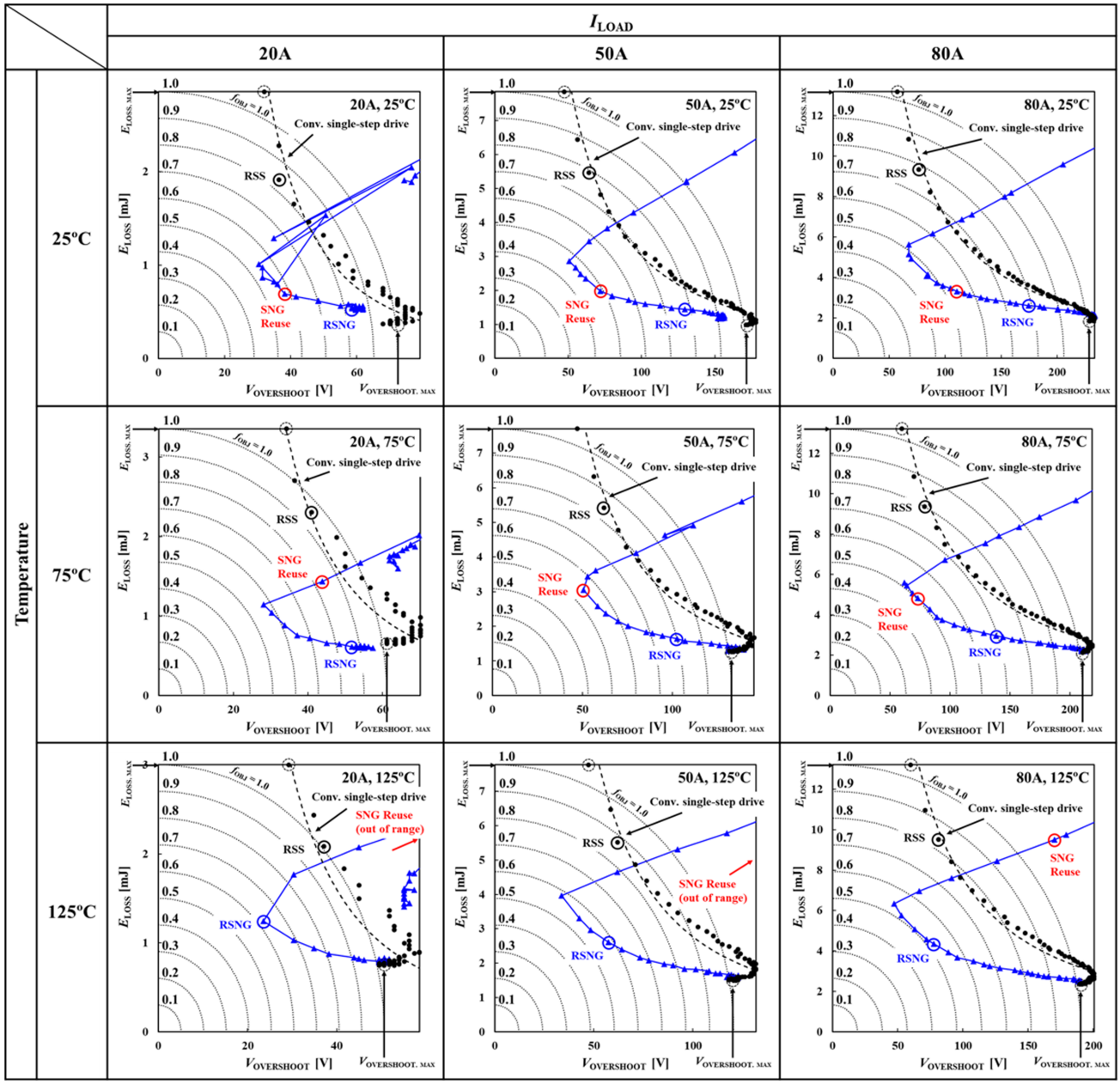

Fig. 13. Measured E_{LOSS} versus $V_{OVERSHOOT}$ of different gate drives in turn-OFF state. Black curves: tradeoff curves of single-step gate drive with varied n. Blue curves: results of stop-and-go gate drive with varied n_2. Black circles: robust single-step gate drive (RSS). Blue circles: proposed robust stop-and-go (RSNG) gate drive. Red circles: reuse of optimum stop-and-go GVs at 50 A, 75 °C (SNG reuse).

from 64 to 10. As a result, the required measurements for a full search in a single condition are reduced from 64^4 to 10^4. In total, the 90 000 ($=9\times10^4$) measurements across nine different conditions take about 5.5 hours. From the measured results, the maximum f_{OBJ}s of the RGVs across nine conditions in turn-ON and turn-OFF state are, respectively, around 0.7 and 0.75.

In [20], a search method of RSA is proposed. Temperature variation is emulated by gate driving current variation, which is realized by adding Δ into GV. The GV becomes $(n_1+\Delta, n_2+\Delta, n_3+\Delta, n_4+\Delta)$ where Δ is 0 or 1, in total 16 ($=2^4$) combinations. An inner loop which is repeated 16 times is added into the SA iteration. Therefore, RGV is searched under a single condition by RSA. It takes about 50 min to search RGV by repeating about 2500 optimization loops ($=2500\times16=40\,000$ measurements). From the measured results, the maximum f_{OBJ_OFF} across different temperature conditions is around 1. However, only temperature variation in turn-OFF state is discussed.

In this article, 63 and 256 ($=4\times64$) measurements are required to search RGVs in turn-ON and turn-OFF states, which take less than 1 and 4 min, respectively. From the measured results, the maximum f_{OBJ_ON} and f_{OBJ_OFF} are 0.75 and 0.87, which show great robustness of RGV from the proposed search method. The comparison between search methods and the performances of different RGVs is given in Table I. Compared with the full

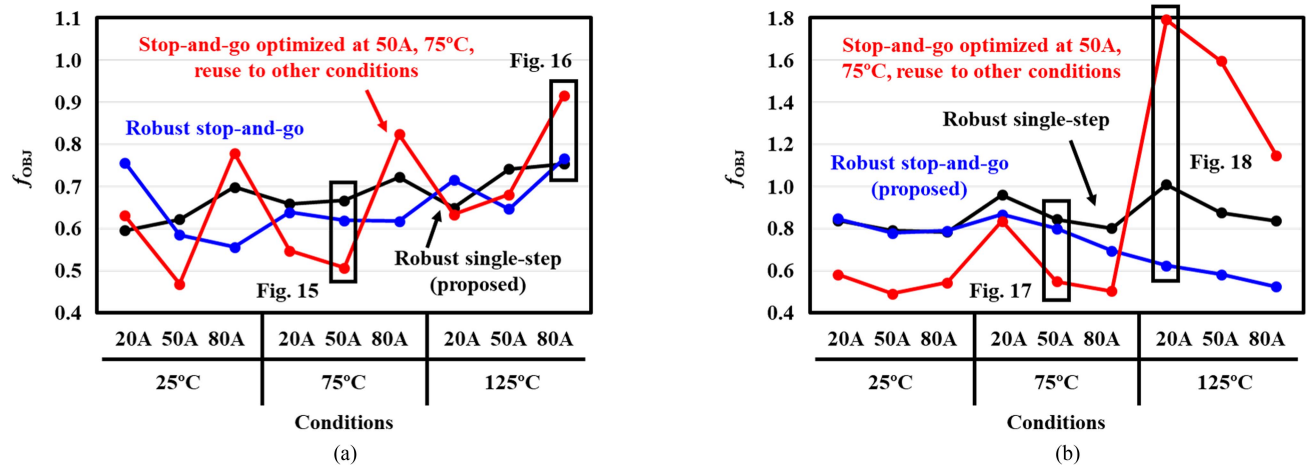

Fig. 14. f_{OBJ} of three gate drives at nine conditions. (a) Turn-ON state. (b) Turn-OFF state.

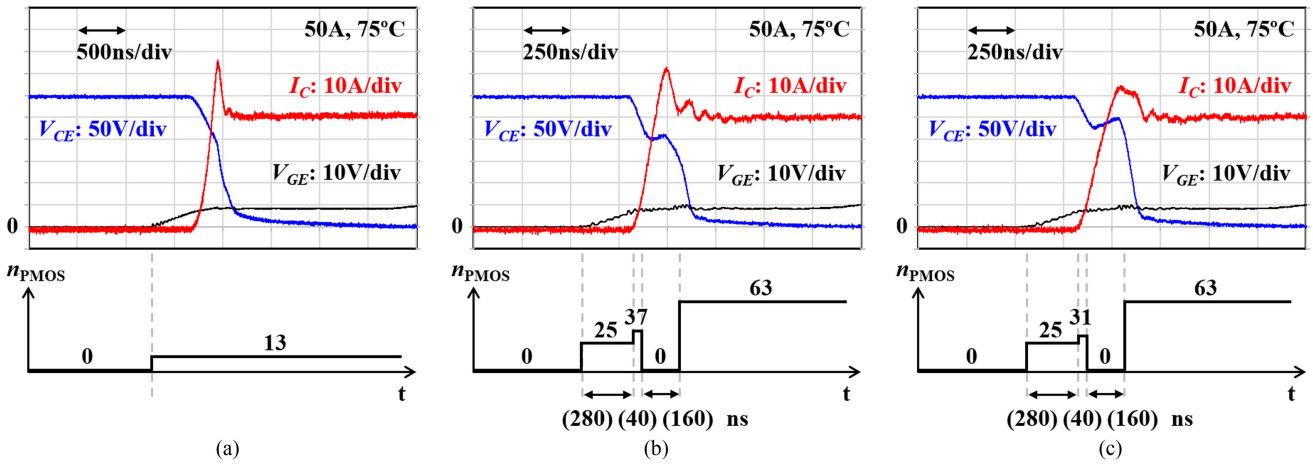

Fig. 15. GVs and measured waveforms at 50 A, 75 °C in turn-ON state. (a) Proposed robust single-step gate drive. (b) Robust stop-and-go gate drive. (c) Optimum stop-and-go gate drive.

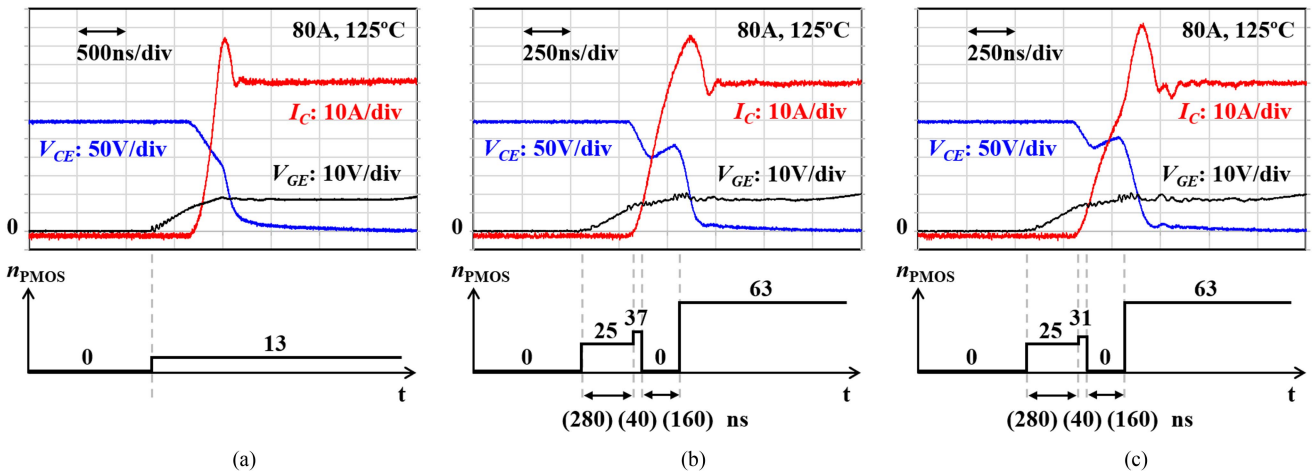

Fig. 16. GVs and measured waveforms at 80 A, 125 °C in turn-ON state. (a) Proposed robust single-step gate drive. (b) Robust stop-and-go gate drive. (c) Reuse of optimum stop-and-go gate drive at 50 A, 75 °C.

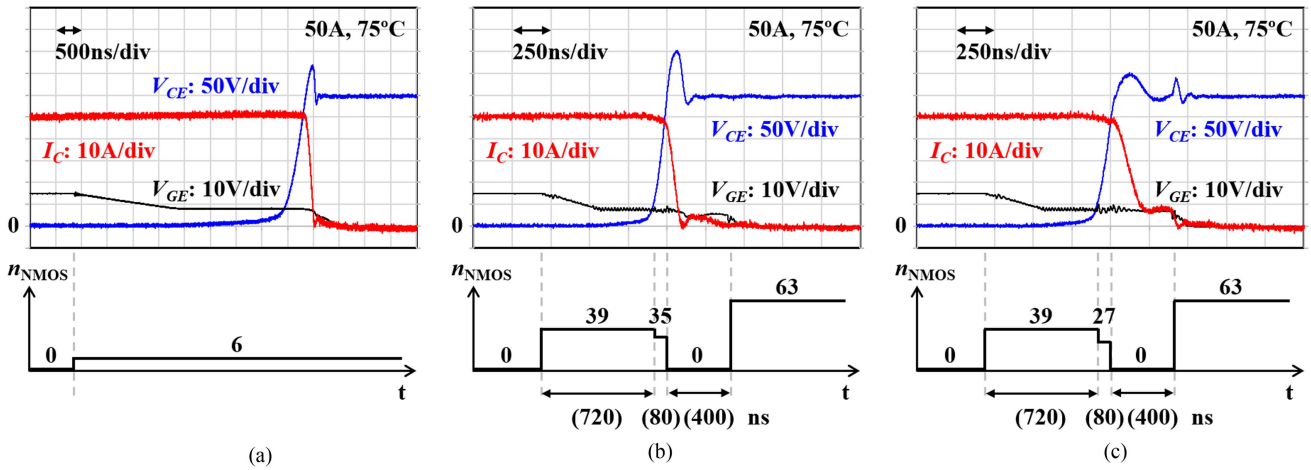

Fig. 17. GVs and measured waveforms at 50 A, 75 °C in turn-OFF state. (a) Robust single-step gate drive. (b) Proposed robust stop-and-go gate drive (c) Optimum stop-and-go gate drive.

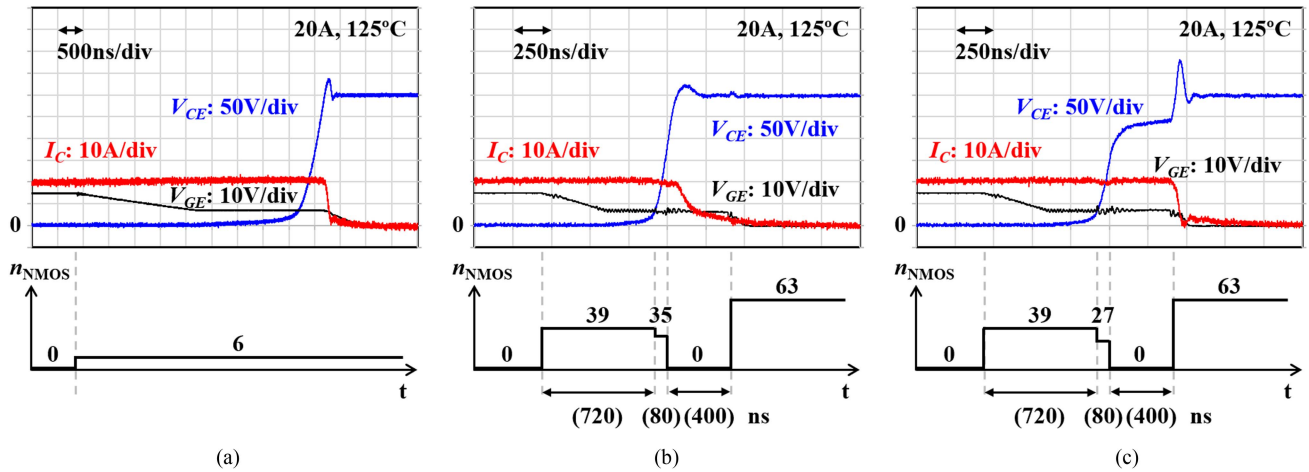

Fig. 18. GVs and measured waveforms at 20 A, 125 °C in turn-OFF state. (a) Robust single-step gate drive. (b) Proposed robust stop-and-go gate drive. (c) Reuse of optimum stop-and-go gate drive at 50 A, 75 °C.

TABLE I
COMPARISON OF STATE-OF-THE-ART RGV SEARCH METHOD AND PERFORMANCE

	Sai et al. [18]	Wang et al. [20]	This article
Search method	Full search	RSA	1 corner (Turn-on) 4 corner (Turn-off)
Required measurements	90 000	40 000	63 (Turn-on) 256 (Turn-off)
Test cost	5.5 h	50 min	1 min (Turn-on) 4 min (Turn-off)
Maximum f_{OBJ}	0.7 (Turn-on) 0.75 (Turn-off)	1 (Turn-off)	0.75 (Turn-on) 0.87 (Turn-off)
Condition variation	I_{LOAD} Temperature	Temperature	I_{LOAD} Temperature

search method of RGV [18], although the maximum f_{OBJ_ON} and f_{OBJ_OFF} are slightly larger, the test cost is greatly reduced by 99%. Compared with RSA [20], not only the maximum f_{OBJ} is lower, but also the test cost can be reduced by 92%.

The searched RGVs in this article are effective to I_{LOAD} and temperature variations. However, when the IGBT's threshold voltage varies due to manufacturing variations, research of RGV is required.

V. CONCLUSION

The test cost of searching RGV against variation in operating conditions is very high. In this article, RGV search methods for both turn-ON and turn-OFF states are proposed to reduce the test cost of searching RGV. In the switching measurements of IGBT at 300 V across the nine operating conditions including different I_{LOAD} (20 A, 50 A, 80 A) and temperature (25 °C, 75 °C, 125 °C), maximum f_{OBJ_ON} and f_{OBJ_OFF} of the searched RGV are 0.75 and 0.87, respectively. Compared with previous works of RGV search methods in [18] and [20], the proposed search method reduces the test cost by 99% and 92% while providing a moderate f_{OBJ}.

REFERENCES

[1] Z. Wang, X. Shi, L. M. Tolbert, F. Wang, and B. J. Blalock, "A DI/DT feedback-based active gate driver for smart switching and fast overcurrent protection of IGBT modules," *IEEE Trans. Power Electron.*, vol. 29, no. 7, pp. 3720–3732, Jul. 2014.

[2] A. P. Camacho, V. Sala, H. Ghorbani, and J. L. R. Martinez, "A novel active gate driver for improving SiC MOSFET switching trajectory," *IEEE Trans. Ind. Electron.*, vol. 64, no. 11, pp. 9032–9042, Nov. 2017.

[3] P. Nayak and K. Hatua, "Parasitic inductance and capacitance-assisted active gate driving technique to minimize switching loss of SiC MOSFET," *IEEE Trans. Ind. Electron.*, vol. 64, no. 10, pp. 8288–8298, Oct. 2017.

[4] P. Nayak and K. Hatua, "Active gate driving technique for a 1200 V SiC MOSFET to minimize detrimental effects of parasitic inductance in the converter layout," *IEEE Trans. Ind. Appl.*, vol. 54, no. 2, pp. 1622–1633, Mar./Apr. 2018.

[5] A. Paredes, E. Fernandez, V. Sala, H. Ghorbani, and L. Romeral, "Switching trajectory improvement of SiC MOSFET devices using a feedback gate driver," in *Proc. IEEE Int. Conf. Ind. Technol.*, 2018, pp. 847–852.

[6] S. Zhao, X. Zhao, A. Dearien, Y. Wu, Y. Zhao, and H. A. Mantooth, "An intelligent versatile model-based trajectory-optimized active gate driver for silicon carbide devices," *IEEE J. Emerg. Sel. Topics Power Electron.*, vol. 8, no. 1, pp. 429–441, Mar. 2020.

[7] S. Zhao et al., "Adaptive multi-level active gate drivers for SiC power devices," *IEEE Trans. Power Electron.*, vol. 35, no. 2, pp. 1882–1898, Feb. 2020.

[8] N. Idir, R. Bausiere, and J. J. Franchaud, "Active gate voltage control of turn-on DI/DT and turn-off dv/dt in insulated gate transistors," *IEEE Trans. Power Electron.*, vol. 21, no. 4, pp. 849–855, Jul. 2006.

[9] L. Dulau, S. Pontarollo, A. Boimond, J.-F. Garnier, N. Giraudo, and O. Terrasse, "A new gate driver integrated circuit for IGBT devices with advanced protections," *IEEE Trans. Power Electron.*, vol. 21, no. 1, pp. 38–44, Jan. 2006.

[10] Y. Yang, Y. Wen, and Y. Gao, "A novel active gate driver for improving switching performance of high-power SiC MOSFET modules," *IEEE Trans. Power Electron.*, vol. 34, no. 8, pp. 7775–7787, Aug. 2019.

[11] Y. Ling, Z. Zhao, and Y. Zhu, "A self-regulating gate driver for high-power IGBTs," *IEEE Trans. Power Electron.*, vol. 36, no. 3, pp. 3450–3461, Mar. 2021.

[12] M. V. Krishna and K. Hatua, "Current controlled active gate driver for 1200V SiC MOSFET," in *Proc. IEEE Int. Conf. Power Electron., Drives Energy Syst.*, 2016, pp. 1–6.

[13] S. Musumeci, A. Raciti, A. Testa, A. Galluzzo, and M. Melito, "Switching-behavior improvement of insulated gate-controlled devices," *IEEE Trans. Power Electron.*, vol. 12, no. 4, pp. 645–653, Jul. 1997.

[14] D. Zhou, K. Sun, Z. Liu, L. Huang, K. Matsuse, and K. Sasagawa, "A novel driving and protection circuit for reverse-blocking IGBT used in matrix converter," *IEEE Trans. Ind. Appl.*, vol. 43, no. 1, pp. 3–13, Jan./Feb. 2007.

[15] F. Zhang, X. Yang, Y. Ren, L. Feng, W. Chen, and Y. Pei, "Advanced active gate drive for switching performance improvement and overvoltage protection of high-power IGBTs," *IEEE Trans. Power Electron.*, vol. 33, no. 5, pp. 3802–3815, May 2018.

[16] M. Takamiya, K. Miyazaki, H. Obara, T. Sai, K. Wada, and T. Sakurai, "Power electronics 2.0: IoT-connected and AI-controlled power electronics operating optimally for each user," in *Proc. IEEE 29th Int. Symp. Power Semicond. Devices ICs*, 2017, pp. 29–32.

[17] T. Sai et al., "Load current and temperature dependent optimization of active gate driving vectors," in *Proc. IEEE Energy Convers. Congr. Expo.*, 2019, pp. 3292–3297.

[18] T. Sai et al., "Robust gate driving vectors to load current and temperature variations for digital gate drivers," in *Proc. IEEE Int. Future Energy Electron. Conf.*, 2019, pp. 87–94.

[19] K. Miyazaki et al., "General-purpose clocked gate driver IC with programmable 63-level drivability to optimize overshoot and energy loss in switching by a simulated annealing algorithm," *IEEE Trans. Ind. Appl.*, vol. 53, no. 3, pp. 2350–2357, May–Jun. 2017.

[20] T.-W. Wang et al., "Automatic search method of robust gate driving vectors for digital gate drivers against variations in operating conditions of IGBT's," in *Proc. IEEE Energy Convers. Congr. Expo.*, 2020, pp. 3798–3802.

[21] T. Sai et al., "Stop-and-go gate drive minimizing test cost to find optimum gate driving vectors in digital gate drivers," in *Proc. IEEE Appl. Power Electron. Conf. Expo.*, 2020, pp. 3096–3101.

[22] H. Kuhn, T. Koneke, and A. Mertens, "Considerations for a digital gate unit in high power applications," in *Proc. IEEE Power Electron. Spec. Conf.*, 2008, pp. 2784–2790.

[23] L. Dang, H. Kuhn, and A. Mertens, "Digital adaptive driving strategies for high-voltage IGBTs," in *Proc. IEEE Energy Convers. Congr. Expo.*, 2011, pp. 2993–2999.

[24] D. Yamaguchi et al., "An optimization method of a digital active gate driver under continuous switching operation being capable of suppressing surge voltage and power loss in PWM inverters," *IEEE Trans. Ind. Appl.*, vol. 58, no. 1, pp. 481–493, Jan./Feb. 2022.

[25] D. Colin and N. Rouger, "High speed digital optical signal transfer for power transistor gate driver applications," in *Proc. IEEE 29th Int. Symp. Power Semicond. Devices ICs*, 2017, pp. 37–40.

[26] H. Dymond et al., "A 6.7-GHz active gate driver for GaN FETs to combat overshoot, ringing, and EMI," *IEEE Trans. Power Electron.*, vol. 33, no. 1, pp. 581–594, Jan. 2018.

[27] Y. Cheng, T. Mannen, K. Wada, K. Miyazaki, M. Takamiya, and T. Sakurai, "Optimization platform to find a switching pattern of digital active gate drive for reducing both switching loss and surge voltage," *IEEE Trans. Ind. Appl.*, vol. 55, no. 5, pp. 5023–5031, Sep./Oct. 2019.

[28] R. Katada et al., "Digital gate driving (DGD) is double-edged sword: How to avoid huge voltage overshoots caused by DGD for GaN FETs," in *Proc. IEEE Energy Convers. Congr. Expo.*, 2021, pp. 5412–5416.

[29] H. Obara, K. Wada, K. Miyazaki, M. Takamiya, and T. Sakurai, "Active gate control in half-bridge inverters using programmable gate driver ICs to improve both surge voltage and switching loss," in *Proc. IEEE Appl. Power Electron. Conf. Expo.*, 2017, pp. 1153–1159.

[30] T. Mannen, K. Wada, H. Obara, K. Miyazaki, M. Takamiya, and T. Sakurai, "Active gate control for switching waveform shaping irrespective of the circuit stray inductance in a practical full-bridge IGBT inverter," in *Proc. IEEE Appl. Power Electron. Conf. Expo.*, 2018, pp. 3108–3113.

[31] H. Obara, K. Wada, K. Miyazaki, M. Takamiya, and T. Sakurai, "Active gate control in half-bridge inverters using programmable gate driver ICs to improve both surge voltage and converter efficiency," *IEEE Trans. Ind. Appl.*, vol. 54, no. 5, pp. 4603–4611, Sep./Oct. 2018.

[32] Y. S. Cheng, T. Mannen, K. Wada, K. Miyazaki, M. Takamiya, and T. Sakurai, "Optimization platform to find a switching pattern of digital active gate drive for full-bridge inverter circuit," in *Proc. IEEE Energy Convers. Congr. Expo.*, 2018, pp. 6441–6447.

[33] Y. S. Cheng, T. Mannen, K. Wada, K. Miyazaki, M. Takamiya, and T. Sakurai, "High-speed searching of optimum switching pattern for digital active gate drive circuit of full bridge inverter circuit," in *Proc. IEEE Appl. Power Electron. Conf. Expo.*, 2019, pp. 2740–2745.

[34] H. Obara et al., "Design and implementation of digital active gate control with variable 63-level drivability controlled by serial 4-bit signals," in *Proc. IEEE Energy Convers. Congr. Expo.*, 2019, pp. 2408–2412.

[35] Y. S. Cheng et al., "Digital active gate drive with optimal switching patterns to adapt to sinusoidal output current in a full bridge inverter circuit," in *Proc. 45th Annu. Conf. IEEE Ind. Electron. Soc.*, 2019, pp. 1684–1689.

[36] T. Mannen et al., "Effect on digital active gate control of a practical IGBT full-bridge inverter with the additional DC-link capacitor close to power devices," in *Proc. IEEE 4th Int. Future Energy Electron. Conf.*, 2019, pp. 1–6.

[37] D. Yamaguchi et al., "Digital active gate control for a three-phase inverter circuit for a surge voltage suppression and switching loss reduction," in *Proc. IEEE Energy Convers. Congr. Expo.*, 2020, pp. 3782–3787.

[38] Y. S. Cheng et al., "High-speed searching of optimum switching pattern for digital active gate drive to adapt to various load conditions," *IEEE Trans. Ind. Electron.*, vol. 69, no. 5, pp. 5185–5194, May 2022.

[39] Y. Sukhatme, V. K. Miryala, P. Ganesan, and K. Hatua, "Digitally controlled gate current source-based active gate driver for silicon carbide MOSFETs," *IEEE Trans. Ind. Electron.*, vol. 67, no. 12, pp. 10121–10133, Dec. 2020.

Ting-Wei Wang (Student Member, IEEE) received the B.S. degree in electronic engineering from National Chiao Tung University, Hsinchu, Taiwan, in 2017. He is currently working toward the Ph.D. degree in electronic engineering with National Yang Ming Chiao Tung University, Hsinchu.

His research interest includes gate driver integrated circuit for wide-bandgap power devices.

Toshiaki Inuma received the B.S degree in electronics and communication engineering from Musashi Institute of Technology, Tokyo, Japan in 1983.

He was with Headquarters Technology Development Department, Hitachi Transport System, Ltd. from 1984 to 2015. He is qualified for Professional Engineer, Japan (electrical/electronics, industrial engineering) and the first-class radio engineer in Japan. Since 2020, he has been a Project Academic Specialist with the University of Tokyo. His research interest includes measurement of digital gate driver circuits for power electronics.

Po-Hung Chen (Senior Member, IEEE) received the M.S. degree in electronic engineering from National Chiao Tung University, Hsinchu, Taiwan, in 2007, and the Ph.D. degree in electrical engineering from The University of Tokyo, Tokyo, Japan, in 2012.

In 2011, he was a Visiting Scholar with the University of California at Berkeley, Berkeley, CA, USA, where he conducted research in fully integrated power management circuits for RISC-V processors. He is currently a Professor with the Institute of Electronics, National Yang Ming Chiao Tung University, Hsinchu, Taiwan. His research focuses on power management integrated circuits, with a special emphasis on energy harvesting, battery management, battery charger, and wireless power transmission.

Dr. Chen has been a Technical Program Committee Member of the IEEE Symposium on VLSI Circuits since 2020 and the IEEE Asian Solid-State Circuits Conference since 2016. He was the TPC Vice-Chair of A-SSCC 2020 and a Guest Editor for IEEE JOURNAL OF SOLID-STATE CIRCUITS. He is also the Vice Chair of the IEEE Solid-State Circuits Society Taipei Chapter.

Makoto Takamiya (Senior Member, IEEE) received the B.S., M.S., and Ph.D. degrees in electronic engineering from the University of Tokyo, Japan, in 1995, 1997, and 2000, respectively.

In 2000, he was with NEC Corporation, Japan, where he was engaged in the circuit design of high speed digital LSI's. In 2005, he was with the University of Tokyo, Tokyo, Japan, where he is currently a Professor with the Institute of Industrial Science. From 2013 to 2014, he was a Visiting Scholar with the University of California, Berkeley, CA, USA. His research interests include the digital gate driver and sensor ICs for power electronics and the integrated power management circuits for automotive and industrial applications.

Dr. Takamiya is a member of the technical program committee of IEEE Symposium on VLSI Circuits and IEEE Asian Solid-State Circuits Conference. He formerly served on the technical program committees of IEEE International Solid-State Circuits Conference (ISSCC) from 2015 to 2020 and IEEE Custom Integrated Circuits Conference from 2006 to 2011. He was a Far East Regional Chair in ISSCC 2020. He was a Distinguished Lecturer of IEEE Solid-State Circuits Society from 2019 to 2020. He was the recipient of 2009 and 2010 IEEE Paul Rappaport Awards and the best paper award in 2013 IEEE Wireless Power Transfer Conference.